remote sensing

MDPI

Article

A Novel ISAR Image Feature Suppression Method Based on Arbitrary Phase Encoding

Yanfeng Wang, Qihua Wu *, Xiaobin Liu, Zhiming Xu, Feng Zhao and Shunping Xiao

State Key Laboratory of Complex Electromagnetic Environmental Effects on Electronics and Information System, National University of Defense Technology, Changsha 410003, China; wangyanfengyf19@nudt.edu.cn (Y.W.); liuxiaobin12@nudt.edu.cn (X.L.); zhimingxu@nudt.edu.cn (Z.X.); zhaofeng321@nudt.edu.cn (F.Z.); xiaoshunping@nudt.edu.cn (S.X.)

* Correspondence: wuqihua13@nudt.edu.cn

Abstract: Compared with the amplitude modulation of conventional interrupted sampling repeater jamming (ISRJ), the image feature control method based on phase modulation exhibits greater energy efficiency and, therefore, has received wide attention recently. In this paper, an Inverse Synthetic Aperture Radar (ISAR) image feature suppression method based on arbitrary phase encoding (APE) is proposed. The parameter design criterion is further analyzed. Through the nonperiodic segmented coding and modulation of the imaging signal in fast and slow time domains, the modulated signal produces a two-dimensional suppression region with uniform energy distribution in the ISAR image. Simulations via the measured Yak-42 aircraft data have verified the effectiveness of the proposed method for target feature control. Compared to binary phase modulation jamming, the APE method with a phase modulation accuracy of 1 degree can achieve the same jamming effect while reducing the jamming power requirement by 3 dB. By optimizing with the proposed method, the image entropy of the interfered image increases by 1.1 to 1.5 compared to the original image.

Keywords: feature suppression; phase modulation; Inverse Synthetic Aperture Radar; blanket jamming

Citation: Wang, Y.; Wu, Q.; Liu, X.; Xu, Z.; Zhao, F.; Xiao, S. A Novel ISAR Image Feature Suppression Method Based on Arbitrary Phase Encoding. *Remote Sens.* **2024**, *16*, 3960. https://doi.org/10.3390/rs16213960

Academic Editors: Dusan Gleich, Liang Zhang, Yanhua Wang, Shunqiao Sun and Pu Wang

Received: 9 September 2024
Revised: 15 October 2024
Accepted: 22 October 2024
Published: 24 October 2024

1. Introduction

Inverse Synthetic Aperture Radar (ISAR) plays a significant role in both civil and military aspects due to its effective monitoring and accurate observation of interested targets with wideband radar signals. Hence, the control of ISAR image features has attracted great attention to protect the targets of interest (TOIs) from being detected and recognized in the past decade [1–3].

Electronic countermeasures are primarily employed to disrupt the target features in ISAR images. ISAR image transform is a unique jamming approach that confuses radar by modulating radar signals in amplitude [4], frequency [5–8], or phase domains, which leads to suppression or deception effects in ISAR images. These effects complicate accurately extracting critical aircraft target features by feature recognition algorithms or deep networks. Then, the TOI can be protected. As a typical amplitude-modulated jamming, interrupted sampling repeater jamming (ISRJ) is widely used due to its ease of implementation and high correlation with the signal. The method modulates and retransmits the radar signal with 0–1 amplitude envelope to produce both deception and suppression jamming effects. However, the intermittent modulation of the amplitude leads to an inefficient utilization of jamming power [9].

Compared with ISRJ, phase modulation shows great potential, as it can continuously modulate in the time domain to ensure that the jamming power is utilized efficiently. However, the research on phase modulation jamming has lagged behind that of amplitude and frequency domain modulations due to the stringent accuracy requirements for modulation. Earlier phase modulation jamming techniques relied on analog devices, resulting in relatively simple suppression patterns and limited control over the uniformity of suppression

effects in the interest areas [10]. Recently, the advancements in Digital Radio Frequency Memory (DRFM) technology and improvements in digital phase modulation accuracy have facilitated the development of phase modulation jamming techniques. Jiang et al. [11], Wang et al. [12], and Sun et al. [13] explored multi-phase modulation in range direction for Linear Frequency Modulation (LFM) radar, pulse compression radar, and other radar regimes. Various optimization criteria have been designed to enhance suppression effects and minimize the risk of being recognized. These ideas are extended to passive surface scenarios [14,15] and multi-base radar electronic countermeasures [16]. However, the application of phase modulation in ISAR countermeasures remains in further development. Yu et al. [17] examined the multi-phase signal modulation jamming mechanism with the rotating platform model of ISAR imaging, identifying eight kinds of suppression effects. Shi et al. applied binary-phase coding to jamming radar images and introduced single-bit modulation with reduced implementation complexity [18]. Both approaches achieved various suppression and deception effects. Another idea is periodic phase coding modulation, which consumes radar resources by setting two-dimensional false targets in ISAR images [16,18,19]. However, the method cannot suppress target features. In our previous work, the concept of coded phase jamming is introduced in [9,20,21]. By employing $0-\pi$ phase modulation rather than the $0-1$ amplitude modulation, the jammer's energy is more effectively utilized to alter radar images. The radar image features can be controlled within specific regions through the design of duty cycle and sub-pulse widths of binary-phase sequences [21]. Through periodic coding with pseudo-random sequences, false targets with irregular amplitude can be set in radar images [9]. Joint modulation in phase and frequency domains offers flexible control over the feature transformation center [20]. Phase modulation jamming demonstrates significant potential and utility for radar image feature control. However, no study has yet explored the jamming potential of multi-phase modulation jamming, and the specific criteria for modulation remain to be discussed.

In this work, the potential of multi-phase modulation jamming is further explored. An ISAR image feature suppression method based on 2D arbitrary phase encoding is proposed to elevate the efficiency of jamming energy. To mitigate the occurrence of energy concentration at isolated points, a Genetic Algorithm (GA) fitness function is proposed to improve the suppression of key features of the target in ISAR images. The effectiveness of the proposed suppression method is validated through simulations with measured ISAR data.

The structure of this paper is organized as follows. Section 2 provides a comprehensive analysis of the signal characteristics and underlying mechanisms of arbitrary phase modulation. In Section 3, the optimization of parameters and the performance metrics employed is discussed. Section 4 presents the results of simulation experiments designed to illustrate the impact of parameter settings on jamming effects and to validate the effectiveness of the proposed optimization criterion across various scenarios. Finally, conclusions and outlooks are made in Section 5.

2. The Proposed Feature Suppression Method Using Arbitrary Phase Modulation

2.1. Signal Characteristic of Arbitrary Phase Modulation

As shown in Figure 1, the arbitrary phase pulse in a fast time domain can be denoted as

$$p(t) = rect\left(\frac{t}{\tau}\right) \otimes \sum_{n=-\infty}^{+\infty} a_n \delta(t - n\tau) = \sum_{n=0}^{N-1} a_n rect\left(\frac{t}{\tau}\right) \otimes \delta(t - n\tau) \tag{1}$$

where t is the fast time variable, τ is the sub-pulse width, $\otimes$ is the convolution operation, $\delta(\cdot)$ is the impulse function, n is the index number of the code, and a_n is the phase modulation sequence in the pulse-width T_p, which is composed of the modulation factor in $\{\exp(j2\pi l/L)|l = 0, 1, \cdots, L-1\}$. One pulse contains N codes; therefore, $N = T_p/\tau$. L is the phase modulation number, which presents the number of phases that can be realized by a digital phase shifter.

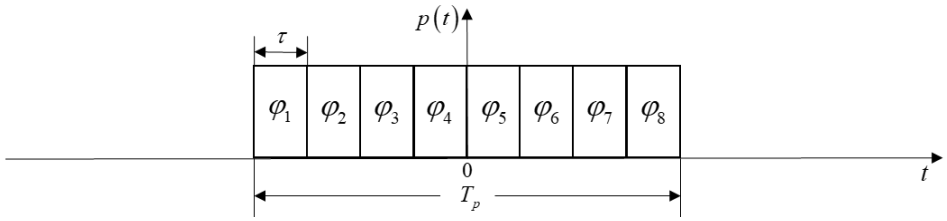

Figure 1. The arbitrary phase pulse.

According to the Fourier transform, we have

$$rect\left(\frac{t}{\tau}\right) \leftrightarrow \tau sa(\pi f \tau) \tag{2}$$

$$\delta(t - n\tau) \leftrightarrow \exp(-j2\pi n\tau f) \tag{3}$$

The frequency spectrum of the modulation pulse can be presented by the frequency spectrum of sub-pulses, since the Fourier transform is linearly addable.

$$\begin{aligned} P(f) &= \sum_{n=0}^{N-1} a_n \tau sa(\pi f \tau) \exp(-j2\pi n\tau f) \\ &= \tau sa(\pi f \tau) \sum_{n=0}^{N-1} a_n \exp(-j2\pi n\tau f) \end{aligned} \tag{4}$$

where $sa(x) = \sin(x)/x$.

From Equation (4), the modulation pulse and the original unmodulated signal have a similar $\sin c(\cdot)$ function in their amplitude envelope, while the zero points are different. The sub-pulse width decides the situation of zero points. After defining the width of the center zero points in the frequency spectrum as the main lobe of suppression, we have

$$B_{main} = 2/\tau \tag{5}$$

The phase modulation sequence also affects the amplitude envelope of the frequency spectrum. In an ideal scenario, the maximum amplitude that can be formed at frequency point f_0 is

$$A_{\max}\Big|_{f=f_0} = T_p sa(\pi f_0 \tau) \tag{6}$$

Similarly, the minimum amplitude is

$$A_{\min}\Big|_{f=f_0} = 0 \tag{7}$$

Suppose that the pulse-width of the phase modulation sub-pulse is $\tau = 10$ μs. The pulse-width of the modulation pulse is $T_p = 100$ μs. The phase modulation sequence a_n is a random sequence generated by MATLAB R2022a. As shown in Figure 2, the amplitude envelope is a modulated $\sin c(\cdot)$ function. The narrower the sub-pulse is, the wider the main lobe of the modulating signal will be. In comparison with the unmodulated frequency spectrum, the energy at the peak $f = 0$ is distributed over a wider frequency band. When the number of sub-pulses is $N = 10$, the main lobe becomes 10 times wider than the original one, which is in accordance with theoretical analyses. Thus, a novel feature suppression method against ISAR can be proposed based on the properties of arbitrary phase modulation.

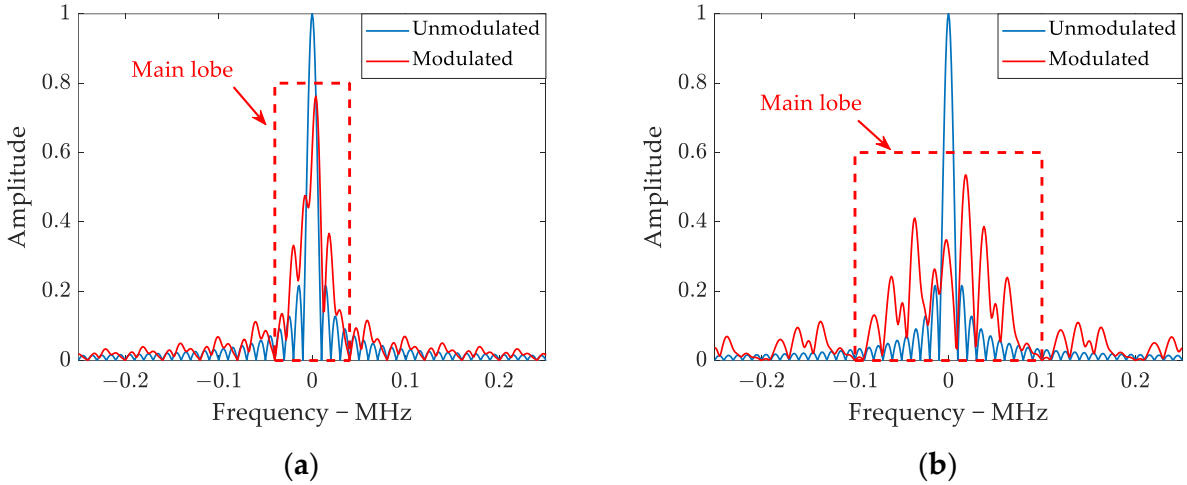

Figure 2. The frequency spectrum of arbitrary phase pulse. (**a**) $N = 4$. (**b**) $N = 10$.

2.2. The Proposed Method

2.2.1. Feature Suppression Signal Model

Figure 3 shows the geometry of the ISAR, the target and the jammer. The local coordinate system xOy is set in the center of target. Assume a scenario in which short-range ISAR is used for the detection of an aircraft target. To prevent the aircraft type from being identified, a jammer is positioned at the aircraft's center, which is the origin O. The range between the radar and the center of target is R_0. ω represents the rotation angular velocity.

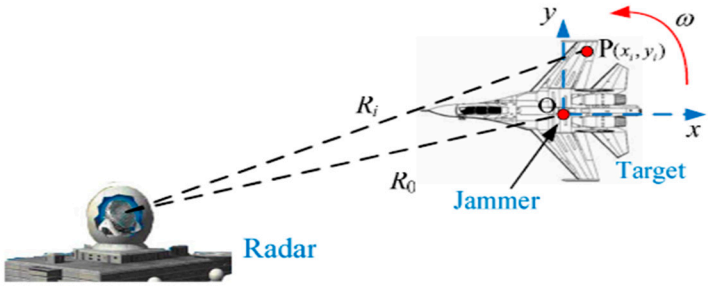

Figure 3. The geometry of the ISAR, the target and the jammer [22].

When ISAR transmits the LFM signal, the radar signal can be given as

$$s(t, t_m) = rect\left(\frac{t}{T_p}\right) \exp\left(j2\pi f_0 t + j\pi k t^2\right) \tag{8}$$

where f_0 is the center frequency, k is the chirp rate, and t_m denotes the slow time variable, where the value is an integer multiple of the pulse repetition interval (PRI), and it satisfies $0 \leq t_m < NT_r$.

Suppose the target is composed of N_T scatter points. The range between the ith scatter point $P(x_i, y_i)$ and radar is

$$R_i(t_m) = R_0 + y_i \cos(\omega t_m) + x_i \sin(\omega t_m) \tag{9}$$

The rotational range during the whole observation time is relatively small in most cases; then, the range R_i is approximated by

$$R_i(t_m) = R_0 + y_i + x_i \omega t_m \tag{10}$$

The echo of the target can be expressed by the sum of each scatter point

$$e(t,t_m)=\sum_{i=1}^{N_T}\left[\begin{array}{l} A_i\cdot rect\left(\dfrac{t}{T_p}\right)rect\left(\dfrac{t_m}{T_A}\right) \\ \cdot\exp\left(j2\pi f_0\left(t-\dfrac{2R_i(t_m)}{c}\right)+j\pi k\left(t-\dfrac{2R_i(t_m)}{c}\right)^2\right)\end{array}\right] \tag{11}$$

where A_i is the amplitude of the ith scatter point, T_A is the total time of imaging, and c is the speed of light.

After matched filtering (MF) or de-chirp in the range direction and fast Fourier transform (FFT) in the azimuth direction, the ISAR image can be given by

$$I(t,f_d)=\sum_{i=1}^{N_T}\left[\begin{array}{l} A_i\cdot\sin c\left(B\left(t-2\dfrac{R_0+y_i}{c}\right)\right) \\ \cdot\sin c\left(T_A\left(f_d-\dfrac{2\omega x_i}{\lambda}\right)\right)\exp\left(-j4\pi\dfrac{R_0+y_i}{\lambda}\right)\end{array}\right] \tag{12}$$

where $\lambda=c/f_0$ is the wavelength of the carrier wave.

After nonperiodic phase modulation in a fast time domain, the modulated radar signal is

$$s_j(t,t_m)=p(t)s(t,t_m). \tag{13}$$

The modulated radar signal, following matched filtering (MF) or de-chirping processing, will exhibit a stretch in the range direction due to the properties of nonperiodic phase modulation. This approach can protect the TOI. However, in the 2D image, this modulation results in multiple bands of suppression, leaving the regions between these bands inadequately suppressed. Arbitrary phase modulation in the slow time domain is proposed to enhance the suppression effect on target features.

The implementation of slow time domain modulation is similar to fast time domain modulation. The sub-pulse width of slow-time domain modulation τ_A is an integer multiple of the PRI. Then, the code number of slow-time domain modulation is $N_A=T_A/\tau_A$. The modulation pulse for the slow-time domain can be expressed as

$$q(t_m)=rect\left(\frac{t_m}{\tau_A}\right)\otimes\sum_{m=0}^{N_A-1}b_m\delta(t_m-m\tau_A) \tag{14}$$

where b_m is the phase modulation sequence, which is composed of the modulation factor in $\{\exp(j2\pi l/L)|l=0,1,\cdots,L-1\}$.

After modulation in the slow-time domain, the modulated radar signal is

$$s_j(t,t_m)=p(t)\cdot q(t)\cdot s(t,t_m) \tag{15}$$

The modulated signal received by the ISAR is

$$y_j(t,t_m)=s_j(t-\tau_0,t_m) \tag{16}$$

where $\tau_0=2R_0/c$ denotes the time delay due to the propagation of electromagnetic waves between the radar and the center of the target.

Assuming that the image of the modulated radar signal is denoted by $I_j(t,t_m)$. The jammed ISAR image is

$$I_{jo}(t,f_d)=I(t,f_d)+I_j(t,f_d) \tag{17}$$

From Equation (17), the output ISAR image is a combination of the target image and the jamming image. To further explore how image features are suppressed, the modulated

radar signal can be deduced without the echoes of the target. In the next section, we will analyze the effects in both range and azimuth directions.

2.2.2. Property in the Range Direction

Assuming that the radar signal at a certain slow time t_m is modulated by an arbitrary phase-coded modulation signal, the modulated radar signal can be represented as

$$x(t) = s(t) \cdot p(t) \tag{18}$$

The frequency spectrum of the modulated radar signal is

$$\begin{aligned} X(f) &= P(f) \otimes S(f) \\ &= \tau sa(\pi f \tau) \sum_{n=0}^{N-1} a_n \exp(-j2\pi n \tau f) \otimes S(f) \end{aligned} \tag{19}$$

where $S(f)$ is the Fourier transform of $s(t)$.

The output of MF is

$$\begin{aligned} y(t) &= \mathcal{F}^{-1}[Y(f)] = \mathcal{F}^{-1}[X(f)S^*(f)] \\ &= \mathcal{F}^{-1}[P(f) \otimes S(f) \cdot S^*(f)] \\ &= \mathcal{F}^{-1}\left[\tau sa(\pi f \tau) S^*(f) \left(\sum_{n=0}^{N-1} a_n \exp(-j2\pi n \tau f) \otimes S(f)\right)\right] \end{aligned} \tag{20}$$

The result of distance-directed MF in Equation (20) is decided by the phase modulation sequence, the sub-pulse width, and the waveform of the radar signal. Due to the properties of MF, the pulse compression result of the modulated radar signal in the range direction is not equal to the sum of the individual sub-pulses after pulse compression. However, since the sub-pulses have the same width, the outputs of their pulse compression take the shape of the $\sin c(\cdot)$ function and have the same zero points, as illustrated in Figure 4a. Therefore, the compression resolution in the range direction can be inferred from the pulse compression resolution of each sub-pulse.

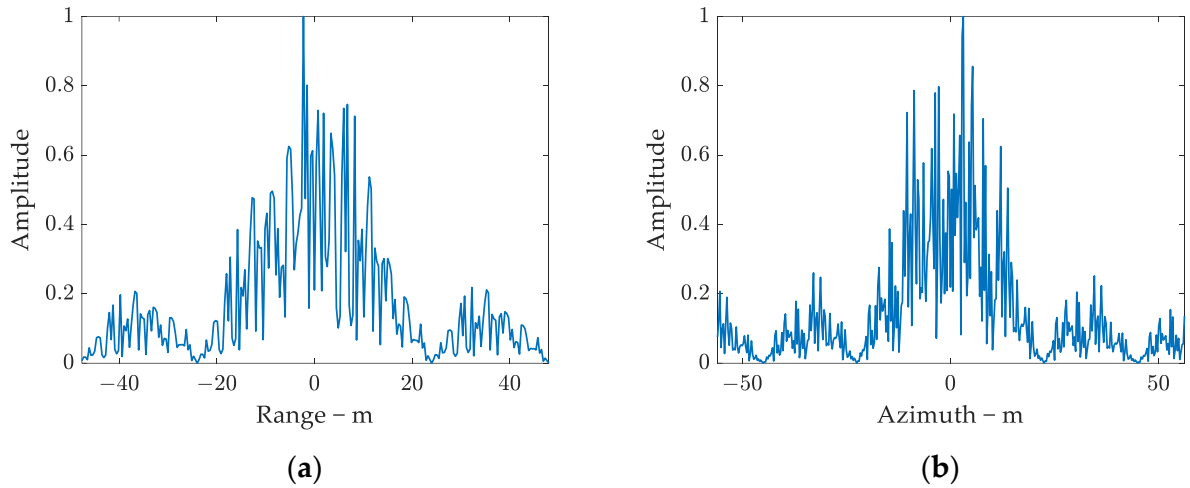

(**a**) (**b**)

Figure 4. Suppression effect of 2D modulation. (**a**) HRRP. (**b**) Azimuth direction slice.

Assuming that the modulation phases of the neighboring sub-pulses are all unequal, for an LFM sub-pulse with a pulse width of τ and a chirp rate of k, the effective bandwidth of range direction pulse compression is

$$B_{sub} = k\tau \tag{21}$$

2.2.3. Property in the Azimuth Direction

The analysis of azimuthal modulation requires an examination in the Doppler frequency domain, as ISAR relies on the rotation speeds of scattering points for azimuthal imaging. Assuming that the radar signal at a certain fast time $s(t_m)$ is modulated by the arbitrary phase-coded modulation signal, it can be represented as

$$x_a(t_m) = s(t_m) \cdot q(t_m) \tag{22}$$

The modulated signal is retransmitted from a single scattering point. Let the Doppler frequency domain be f_d. According to the properties of Fourier transform, the spectrum after azimuth direction modulation is

$$X(f_d) = S(f_d) \otimes Q(f_d) = \delta(f_d) \otimes Q(f_d) = Q(f_d) \tag{23}$$

The effect of azimuth direction modulation is determined by the spectrum of the modulating pulse, which has been analyzed in Equation (5). The output envelope is similar to the $\sin c(\cdot)$ function. The amplitude range of a single resolution can reach $[0, T_p sa(\pi f_0 \tau)]$ through designation of the phase modulation sequence. For each range cell, the modulation effects of azimuthal defocusing are the same.

2.2.4. The Flow Chart of the Proposed Method

A typical scenario of jamming is given in Figure 5a. The TOI passively scatters radar electromagnetic waves as the ISAR images the TOI. At the same time, the TOI recovers the radar signal. The jammer then actively modulates and retransmits the intercepted signal. The ISAR receives both the TOI echo and the jamming signal. The process of the proposed modulation method can be concluded as steps in Figure 5b. Here, a_n is the phase modulation sequence in the range direction, and b_m is the phase modulation sequence in the azimuth direction.

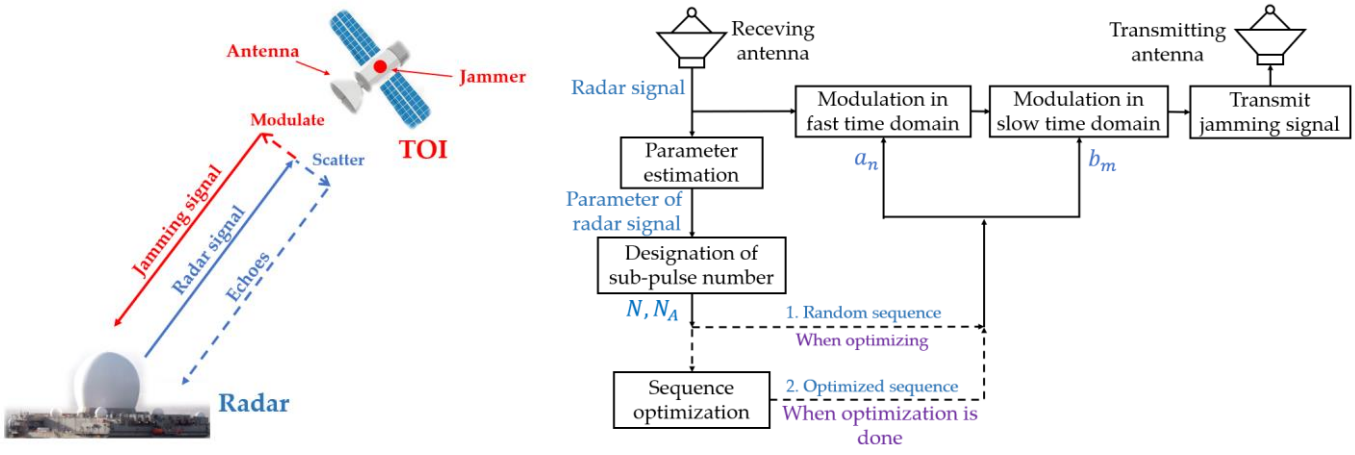

Figure 5. The process of APE jamming. (**a**) The typical scenario of jamming. (**b**) Modulation process of radar signals by the jammer.

Firstly, the receiving antenna intercepts and receives ISAR signals in DRFM.

Then, the intercepted signals will be delivered to two branches. The function of the first branch is to design coding sequences. The parameters of radar signals are estimated to calculate the code width and optimize sequences a_n and b_m. When the coding sequence optimization iteration has not been completed, the jamming signal is modulated with a randomly generated sequence. Since the code width is calculated, the suppression area can be given. Then, in the second branch, the real-time saved radar signals will be multiplied by the phase modulation factor in the fast and slow time domain.

Finally, the modulated radar signals are transmitted in the direction of ISAR as jamming signals. After image processing, ISAR will receive images contaminated by suppression jamming.

3. Feature Suppression Performance Evaluation and Parameter Design

In this section, parameter design guidelines are proposed to ensure the effectiveness of feature suppression, and metrics for evaluation are established.

3.1. Performance Evaluation for Feature Suppression

3.1.1. Suppression Area

The range direction coverage of the suppression can be calculated by the resolution formula for pulse compression

$$\Delta R_R = \frac{c}{B_{sub}} = \frac{c}{k\tau} = \frac{Nc}{kT_p} \tag{24}$$

The azimuth direction coverage of the suppression can be expressed by substituting Equations (5) and (23) into the azimuthal resolution formula

$$\Delta R_A = \frac{\lambda}{\omega\tau_A} \tag{25}$$

The section of the jamming area is

$$\Delta S = \Delta R_R \cdot \Delta R_A = \frac{c\lambda}{k\omega\tau\tau_A} \tag{26}$$

In Equation (26), the feature suppression range of the ISAR image is mainly determined by sub-pulse widths τ and τ_A. The larger the coverage range, the smaller the required sub-pulse width. Due to the main lobe energy conservation, the increase in suppression range may lead to the decrease in the accumulated jamming power in the coverage area and the loss of suppression effect.

3.1.2. Image Entropy

Image entropy [23] is a statistical characterization of the visual features of an image, reflecting the volume of information in the image. One of the definitions is

$$E(I) = -\sum_{\alpha=1}^{A}\sum_{\beta=1}^{B} D(\alpha,\beta)\ln[D(\alpha,\beta)] \tag{27}$$

where $D(\alpha,\beta)$ is the normalized image calculated by

$$D(\alpha,\beta) = \frac{|I(\alpha,\beta)|^2}{\sum\limits_{\alpha=1}^{A}\sum\limits_{\beta=1}^{B}|I(\alpha,\beta)|^2} \tag{28}$$

where $I(\alpha,\beta)$ is the pixel intensity of the original image.

In ISAR application scenarios, background noise is usually low. Suppression jamming disrupts radar imaging by introducing a significant amount of extra error information into

a well-focused target area, which confuses the recognition effect. Images with better focus typically have lower entropy values, while images with better suppression effects have larger image entropy.

3.1.3. Peak Jamming-to-Signal Ratio (PJSR)

The jamming-to-signal ratio is a critical metric for assessing the relationship between the energy of jamming and the echo of radar signals. When it comes to active jamming, the jammer's peak power limits the strength of the jamming directly. As for the target echo, the amplitude of scatter points varies. Using the peak power as a reference makes it easier to analyze the different effects of feature suppression. The peak jamming-to-signal ratio is defined as

$$r_P = \frac{P_{jPeak}}{P_{sPeak}} \tag{29}$$

where P_{jPeak} represents the peak power of the jamming signal, and P_{sPeak} represents the peak power of the echo.

3.2. Parameter Design and Optimization

3.2.1. Sub-Pulse Width Design

Equations (24) and (25) show that the narrower the sub-pulse width, the larger the suppression range. However, the wider range causes lower average jamming power in the interested area. The choice of area size should consider a combination of target size and jamming power. The area of jamming should be larger than the target size to effectively suppress the features of the TOI. It is assumed that the range direction suppression length is L_R, and the azimuth direction suppression length is L_A. The range of the feature suppression region needs to be satisfied

$$\Delta R_R \geq L_R \tag{30}$$

$$\Delta R_A \geq L_A \tag{31}$$

Substituting into Equations (24) and (25), the sub-pulse width needs to be satisfy

$$\tau \leq \frac{c}{kL_R} \tag{32}$$

$$\tau_A \leq \frac{\lambda}{\omega L_A} \tag{33}$$

In engineering applications, the sub-pulse width is constrained by the phase switching time t_{switch} of the digital phase shifter and should satisfy

$$\tau \geq t_{switch} \tag{34}$$

$$\tau_A \geq t_{switch} \tag{35}$$

To concentrate the energy more effectively, the sub-pulse width should be set to its maximum value while adhering to the conditions outlined in Equations (32)–(35). If these equations cannot be simultaneously satisfied, priority should be given to using the phase switching time as the sub-pulse width in the range direction.

3.2.2. Phase Modulation Sequence Optimization

Once the sub-pulse width and the number of code elements for a given radar waveform are determined, the image of the suppression area is solely affected by the sequence of code elements.

The accuracy of a digital phase shifter decides the value of the sub-pulses, which also determines the permutation number of phase modulation sequences. Assume that

the phase shifter is capable of achieving L kinds of phases in a cycle. If the number of range direction sub-pulses is N, and the number of azimuth direction sub-pulses is N_A, there are $L^N \times L^{N_A}$ kinds of possible jamming effects. Thus, phase shifters require higher modulation accuracy to achieve a greater suppression. On the other hand, the computational complexity of traversing the coding sequences increases exponentially. Each iteration requires performing ISAR imaging with range-direction de-chirp and azimuth-direction FFT. The total number of calculations for a single image is $N_r \times N_p + N_r \times N_a \log_2 N_a$ additions and $N_r \times N_p + N_r \times N_a \log_2 N_a$ multiplications. Here, N_r represents the number of range-domain samples, N_a represents the number of azimuth-domain samples, and N_p represents the number of transmitted pulses. To reduce the computational demands of searing through the solution space, an image feature suppression method based on GA is proposed.

Optimization algorithms can convert the problem into a multi-parameter sequential optimization problem. Genetic Algorithms (GAs) [24] are search algorithms that emulate the principles of natural selection and genetics. They optimize the solution space by simulating genetic, crossover, and mutation operations akin to biological evolution, improving the fitness function. The algorithm can handle complex nonlinear problems effectively, offering improved global search capability and robust variations that reduce the risk of converging to a local optimum. It has been widely applied in radar jamming waveform design. Compared to exhaustive search methods, the application of GA can reduce the number of computations required for parameter optimization, but it does not alter the size of the solution space. As the range of the solution space expands, the number of optimization iterations needs to be increased accordingly. Signals with the same power but different encoding methods can maintain similar energy within their main lobes. To enhance the performance of feature suppression, it is crucial to minimize the energy peaks as much as possible. The maximum of the variant jamming image $I_j(t, f_d)$ is used as the fitness function of the optimization algorithm, which can be iterated to obtain a sequence that produces a more uniform suppression effect. The steps of the optimization method for APE feature suppression sequences are illustrated in Figure 6. To enhance the feature suppression effect under low PJSR conditions, the optimization targets the ISAR image produced by the modulated radar signal. Consequently, the optimization process does not consider target features other than size.

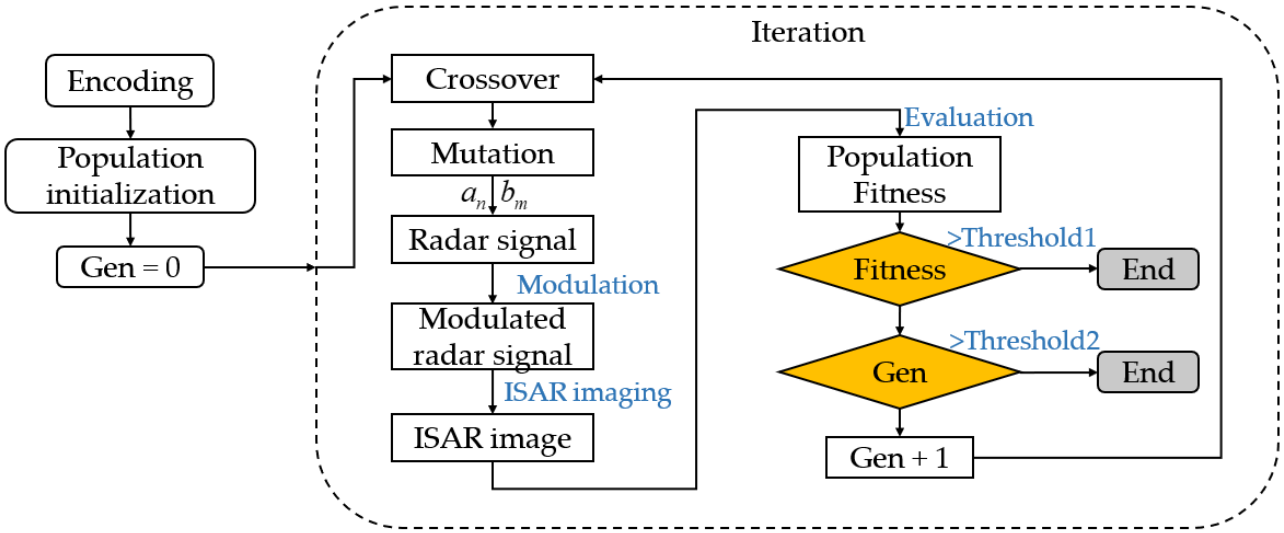

Figure 6. The process of phase modulation sequence optimization based on GA.

Step 1: Encoding

Each sequence value serves as a gene for a chromosome, and each gene is $l \in [0, L-1]$, while the corresponding phase modulation factor is $\exp(j2\pi l/L)$.

Step 2: Population Initialization

Multiple random sequences of length $N + N_A$ with uniformly distributed integer elements in the range of $[0, L-1]$ are generated to obtain the optimized initial population.

Step 3: Iteration

The de-chirp algorithm in the range direction and the FFT algorithm in the azimuth direction are used to compute the ISAR image of the modulated radar signals in the suppression region, setting the fitness of each chromosome within the population to $fitness = 1/\max[I_j(t, f_d)]$. Chromosomes with lower fitness within the population are eliminated. It is judged whether the convergence effect meets the requirement, and if it does not, the iterative loop is continued until the maximum number of iterations is reached. Crossover is performed between chromosomes, individually coded random mutations are performed, and offspring chromosomes are added to the population to continue the iteration.

Step 4: Choose the Optimal Solution

After completing the iterations, the chromosome with the largest fitness function is selected as the optimized phase modulation sequence in the output population.

Since the number of populations and the number of iterations is limited, the GA algorithm iterates to obtain the optimal solution for the iterated populations. As the number of iterations increases, the result will be close to the global optimal solution. It should be noted that the genetic algorithm optimization solution is not unique, so its coding sequence has diversity.

4. Simulation Result

4.1. Simulation Scene Description

In this section, the measured ISAR dataset of a Yak-42 aircraft is conducted to demonstrate the performance of the proposed method. The aircraft is 36.8 m long with a wingspan of 34.9 m. The data are measured by a C-band radar (5.52 GHz) with the bandwidth of 400 MHz. Pulse width $T_p = 25.6$ μs, pulse repetition frequency PRF = 100 Hz, and 400 slow time echoes are taken for the simulation. The range direction sampling number is 256. Thus, the range resolution is 0.375 m. The target ISAR image without jamming is shown in Figure 7. To conduct the proposed jamming method, the coordinate of the active jammer is $(0, 0)$. The experiments in this section were conducted on a platform equipped with an Intel 13900H CPU, 16 GB of RAM, and an NVIDIA RTX 3050Ti GPU. The code was executed using MATLAB R2022a.

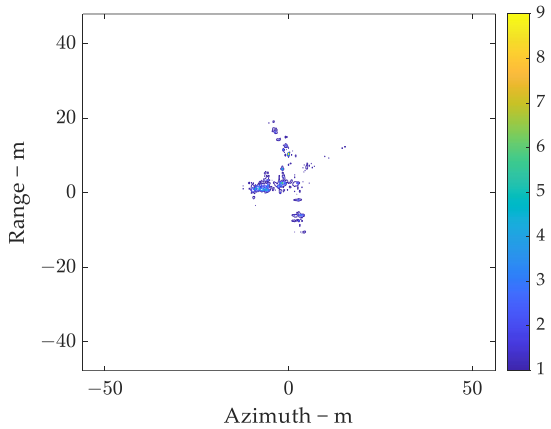

Figure 7. The ISAR image of Yak-42 without jamming, image entropy = 6.8857.

4.2. Feature Suppression Performance Evaluation

4.2.1. Jamming Performance with Various Code Widths

In this subsection, the modulation effect of code width (i.e., the coding number) is demonstrated. The main lobe width must exceed the size of the target in both the range

and azimuth direction according to the principle discussed in Section 3. In this scene, the code width should satisfy $\tau \leq 0.52$ µs and $\tau_A \leq 64.4$ms. Consequently, the coding numbers should satisfy $N \geq 50$ and $N_A \geq 63$, respectively. Figure 8 presents the jamming results with different coding numbers. The PJSR is set at -3 dB, and the phase modulation accuracy is set at 1°.

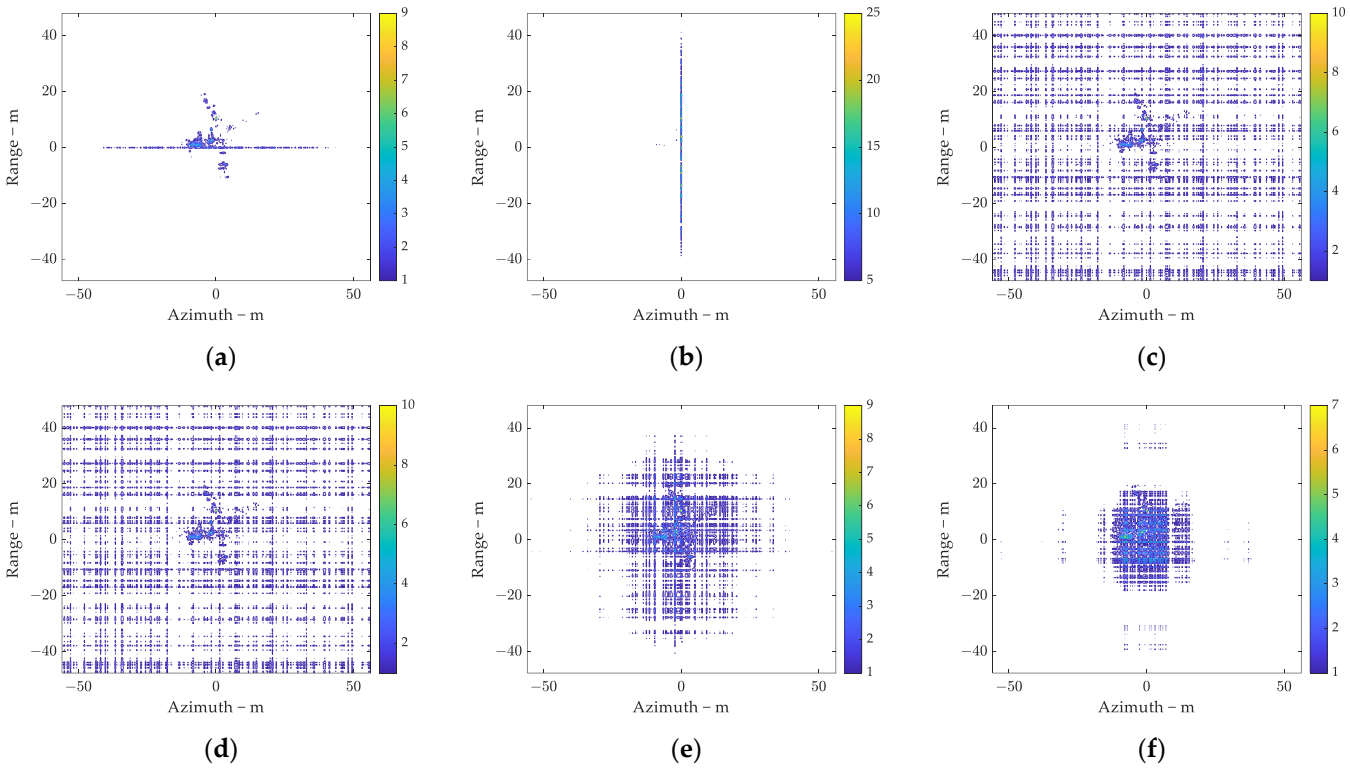

Figure 8. The jamming results with various coding numbers. (**a**) $N = 1$, $N_A = 200$. (**b**) $N = 128$, $N_A = 1$. (**c**) $N = 256$, $N_A = 400$. (**d**) $N = 128$, $N_A = 200$. (**e**) $N = 128$, $N_A = 160$. (**f**) $N = 64$, $N_A = 80$.

As shown in Figure 8a,b, modulation in one dimension produces only a single strip, which is insufficient to cover the features adequately. In Figure 8c–f, the parameters N and N_A satisfy the previous inequality, and the image entropy increased from 6.8857 to 8.2551 by phase modulation jamming. As the coding number increases, the power of the main lobe decreases and becomes more decentralized, making it easier to recognize the target features. The coding number should be as large as possible while satisfying the formula in Section 3.2.1. In this section, the coding numbers $N = 64$ and $N_A = 80$ are suitable for this scenario.

4.2.2. Jamming Performance with Various PJSR

In this subsection, the jamming performance with various PJSRs is presented. The coding number is set as $N = 64$, $N_A = 80$. The main coverage of the jamming measures approximately 48 m in the range direction and 45 m in the azimuth direction, which is consistent with the previous analyses. In Figure 9, with increasing jamming power, the shape and contours of the target become less visible. At the same time, the number of strong scattering points in the target area rises, significantly altering the original relationships between the strong scattering points. At this point, the original scattering structure of the target cannot be restored from the image by adjusting the display range, demonstrating that higher signal power enhances the jamming effect. When $PJSR \geq 0$dB, the strong scattering points are distributed throughout the rectangular coverage area and the position

of the original strong scattering point has shifted, making the shape characteristics of the aircraft indistinguishable, which ensures effective suppression.

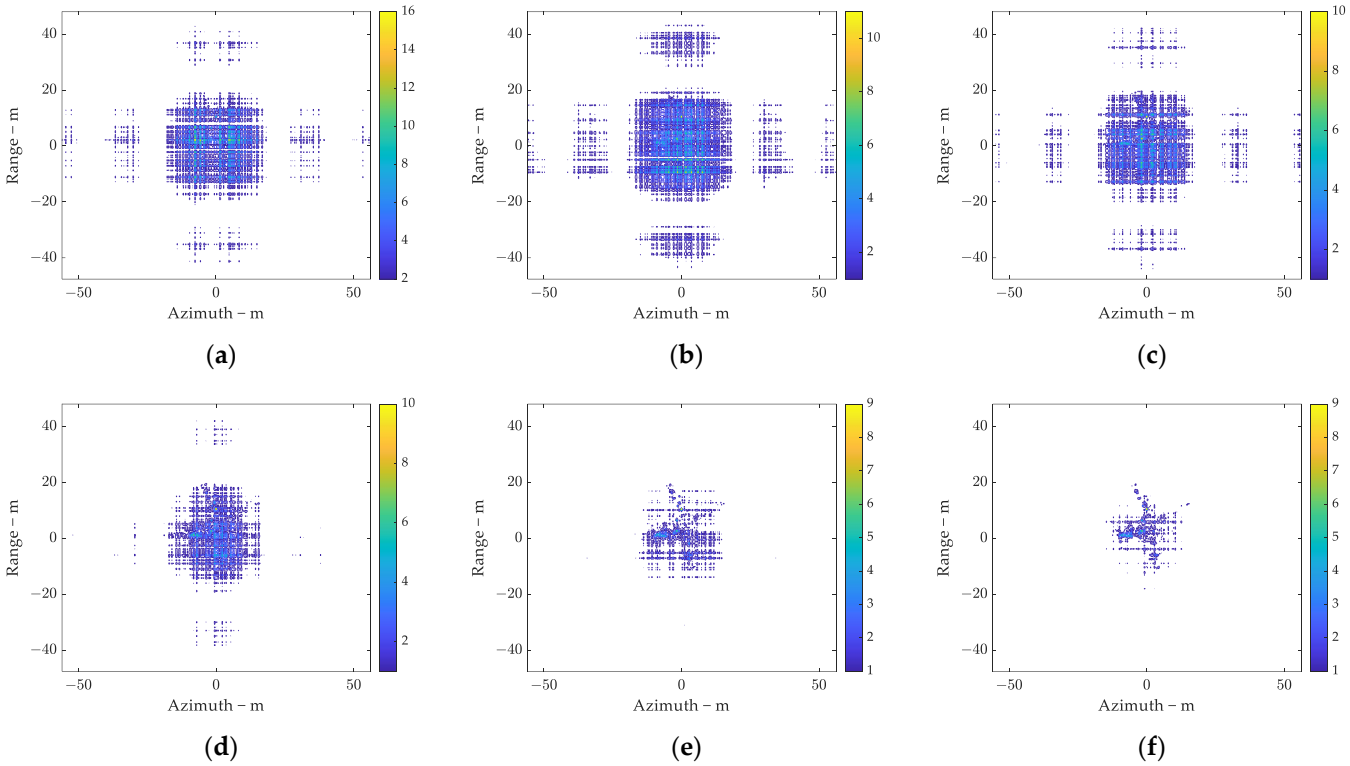

Figure 9. The jamming results with various PJSRs. (**a**) PJSR = 6 dB. (**b**) PJSR = 3 dB. (**c**) PJSR = 0 dB. (**d**) PJSR = −3 dB. (**e**) PJSR = −6 dB. (**f**) PJSR = −9 dB.

The increase in jamming power will lead to a greater impact of the interfered image on each pixel value. Theoretically, when the jamming power is much higher than the target echo power, the resulting image will be the same as the jamming signal alone in ISAR. Therefore, increasing the peak power of the jamming signal is the most direct and effective method to enhance feature suppression.

4.2.3. Analyses for Optimization of Coding Sequence

In previous experiments, phase modulation sequences were generated randomly, leading to variability in suppression performance. To evaluate the impact of optimization, a comparison is made between the proposed optimization method and the random sequence approach.

The modulation parameters are set as $N = 64$, $N_A = 80$ based on the conclusions of the previous experiment. Consequently, the length of each chromosome in each iteration is 144, and the maximum iteration count is set to 100. The optimized jamming signal is applied to the target echoes, and then a de-chirp process is performed in the range direction, which is followed by FFT in the azimuth direction to obtain the interfered image. To quantify the performance of suppression, the image entropy of the target area in the final ISAR image is used. It should be noted that the echoes of the target are not utilized during the iteration, as they cannot be directly intercepted.

As illustrated in Figures 10 and 11, the optimization method enhances the average power of the suppression area in both the range and azimuth direction. The randomly generated modulation sequences cannot suppress the target features effectively because the jamming power is concentrated at individual extreme points. Thus, the jamming power in most of the main lobe area is suppressed. Figures 10 and 11 show that the proposed optimization method results in a target with more blurred outlines. The distribution of jam-

ming energy in the 2D main lobe area becomes more uniform, and the target features on the edge are vaguer. This demonstrates the effectiveness of the proposed optimization method.

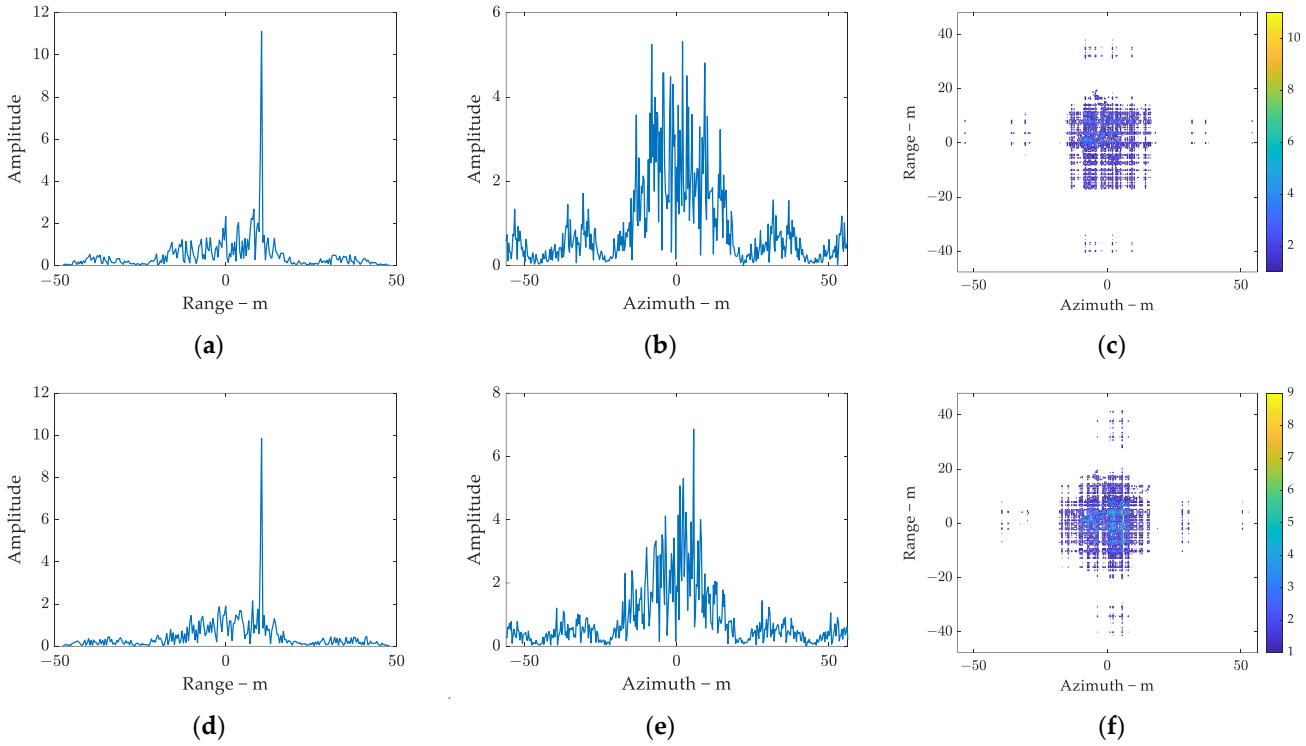

Figure 10. The comparison of optimized jamming and random jamming, PJSR = −3 dB. (**a**–**c**) The interfered ISAR image of the optimized sequence. (**d**–**f**) The interfered ISAR image of the random sequence.

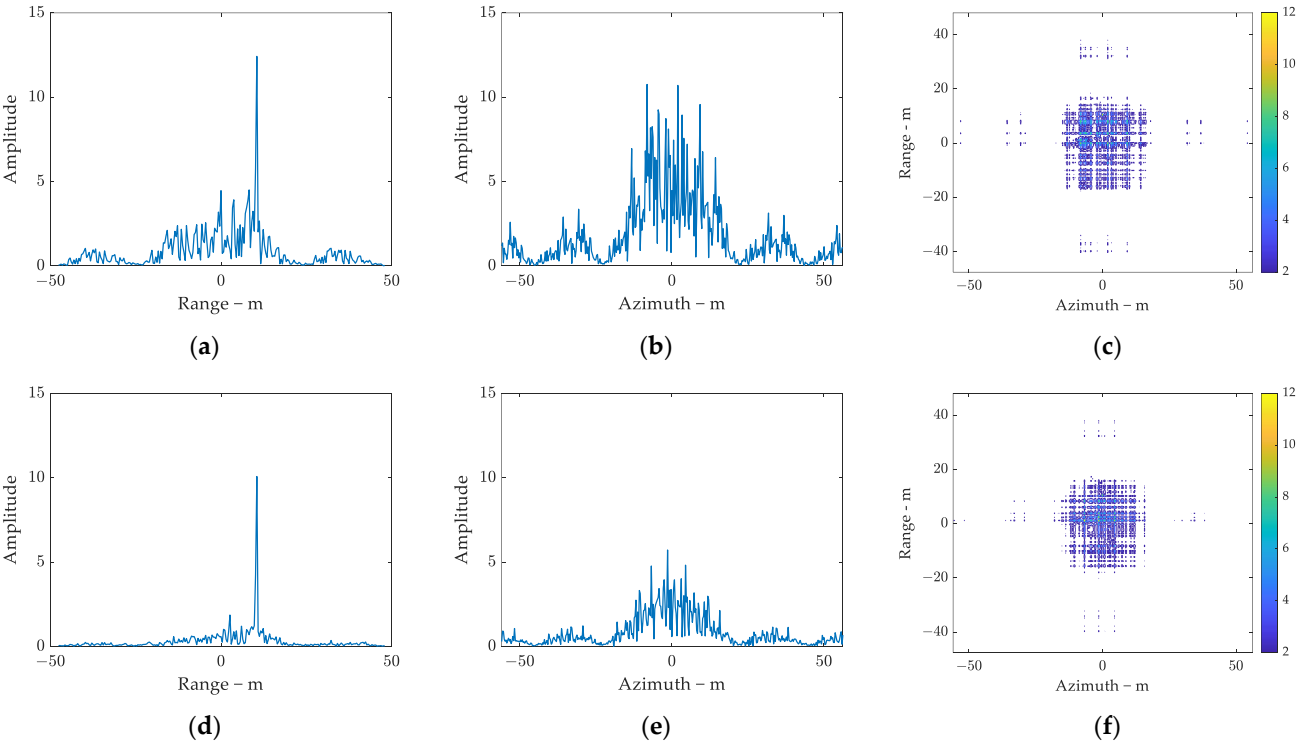

Figure 11. The comparison of optimized jamming and random jamming, PJSR = 3 dB. (**a**–**c**) The interfered ISAR image of the optimized sequence. (**d**–**f**) The interfered ISAR image of random sequence.

Optimizing the coding sequences under various PJSR conditions using the proposed method, Figure 12 illustrates the image entropy of the ISAR image. In the figure, the data shown in red represent the result of the optimized ISAR image, while the other scatters display the distribution of 100 random coded results. As observed, a larger PJSR value increases the image entropy of the optimized image. The optimization consistently achieves results in the top 25% compared to the random results. This demonstrates that the proposed optimization criterion is effective and appropriate.

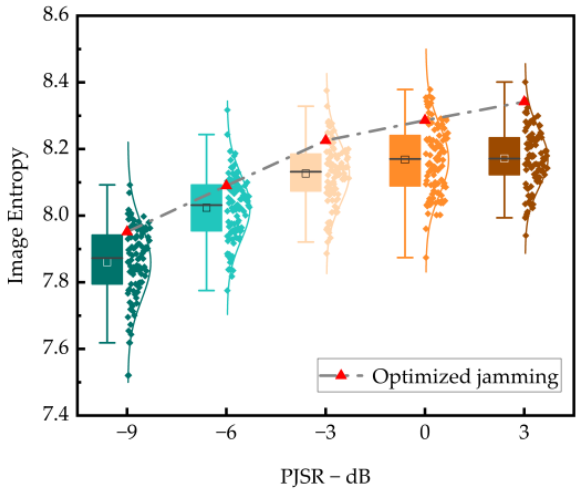

Figure 12. Distribution of image entropy with various coding sequences.

4.2.4. Comparison of the Proposed Method and Binary Phase Modulation

The previous analysis suggests that increasing the phase modulation number may reduce the need for jamming power. This subsection presents a simulation experiment that demonstrates this improvement.

The scene and parameters are set as described in Section 4.3. To assess the jamming performance boundary, phase-modulated radar signals are added directly to the measured ISAR data during the iteration process. The fitness function of the GA is evaluated based on image entropy. Figure 13 displays the maximum image entropy achieved with various phase modulation numbers. The jamming performance of the proposed method is superior to the binary phase modulation when PJSR > −9 dB. Specifically, to achieve a comparable suppression effect, the proposed method requires a PJSR that is 3 dB lower than that required for binary phase modulation, effectively halving the jamming power needed.

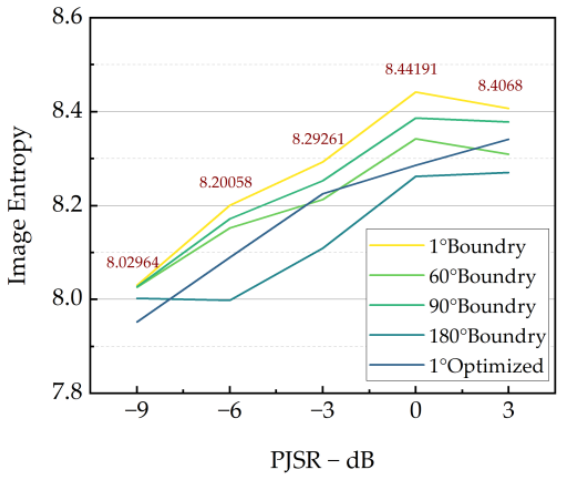

Figure 13. Performance boundaries of different phase modulation numbers.

Furthermore, the relationship between the curves in Figure 13 indicates that increasing the phase modulation number raises the image entropy. This emphasizes that the modulation precision of the digital phase shifter directly constrains the choice of sub-pulse width in such situations. On the other hand, improving the modulation precision increases the optimization solution space, which raises computational power requirements. Therefore, the selection of the actual phase modulation number should be analyzed in conjunction with the computational capacity of the equipment. When the PJSR is less than -9 dB, the effects of arbitrary phase modulation and binary phase modulation are similar. In this scene, the jamming performance saturates when PJSR exceeds 0 dB.

4.3. Comparison with Nonperiodic ISRJ

In this section, we will expand our investigation by comparing the proposed method with a conventional jamming technique. Our focus will be on evaluating the jamming-to-signal ratio (JSR) and image entropy as metrics. The objective is to demonstrate the improvements offered by our method over traditional approaches in the context of radar image jamming.

4.3.1. Experimental Settings

ISRJ, known for its relatively low implementation complexity, has been widely used in radar countermeasures. In radar image jamming, nonperiodic ISRJ can achieve partial coherent gain while producing a suppression effect similar to the proposed method in two-dimensional radar images [22]. For the experiments in this section, we kept the previous jamming parameters constant to compare the jamming effects with different PJSRs.

The ISRJ method includes sampling the radar detection signal, segmenting it, and then amplitude-modulating it with a $0-1$ sequence in the time domain before transmission. Apart from the influence of the modulation object and the encoding sequence, the ways in which the encoding width and jamming power affect the jamming effect are similar. The jamming parameters set in the experiment are detailed in Table 1.

Table 1. Simulation parameters.

Parameter	**Method**	
	APE	**ISRJ**
coding number in range direction	64	64
coding number in azimuth direction	80	80
modulation sequence	random multi-valued sequence	random binary sequence
minimum modulation phase	1°	-
duty cycle	-	0.5 (in range direction) 0.5 (in azimuth direction)
object of modulation	phase	amplitude
number of simulations	100	100

4.3.2. Analyses of Jamming Performance

In this sub-section, we conduct simulation experiments under various PJSR conditions to compare the jamming effects. The jamming images in Figure 14 visually display the differences in jamming effects. One hundred Monte Carlo simulations are performed in this section, allowing for a quantitative description of the differences in imaging results between the two jamming methods. It should be noted that the peak power of the time-domain signals for ISRJ and the proposed method was set to be the same in the experiment to simulate the real jamming machine's peak power limit.

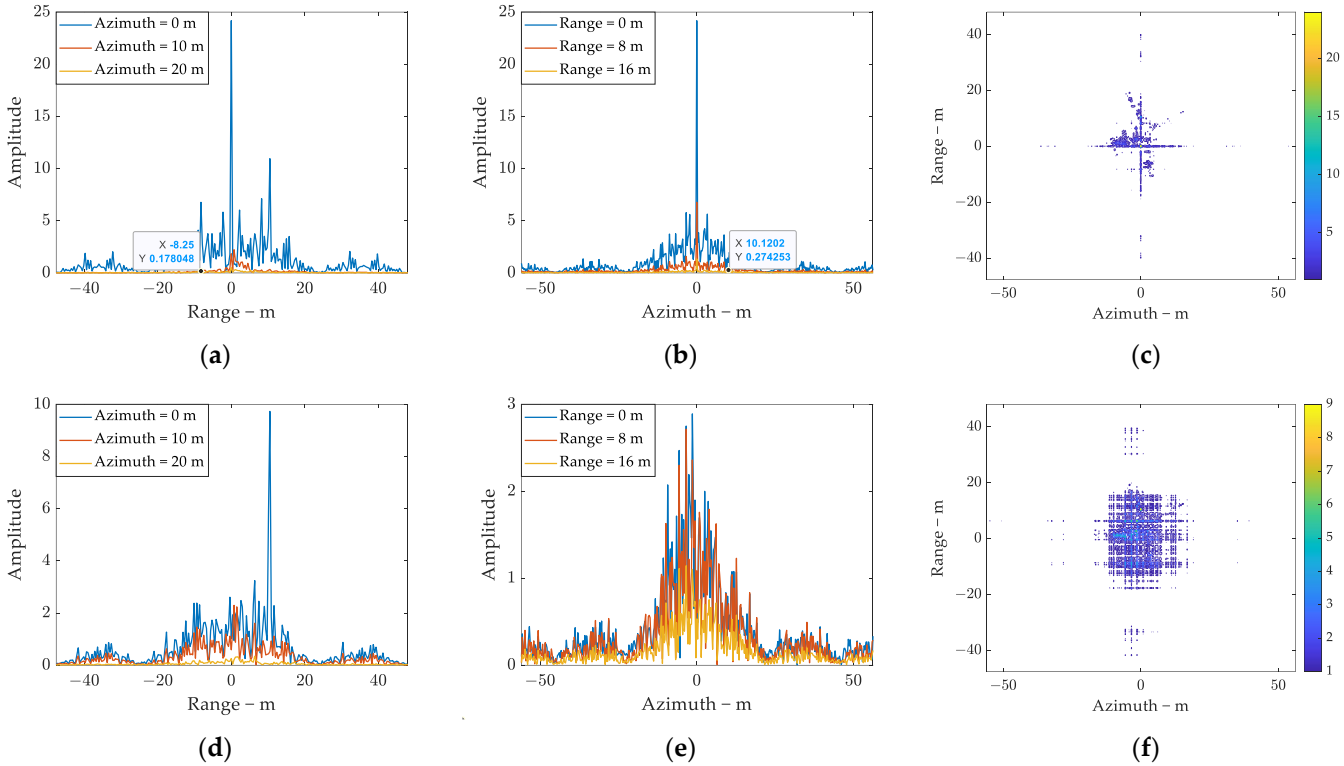

Figure 14. The comparison of nonperiodic ISRJ and APE, PJSR = −3 dB. (**a**–**c**) The interfered ISAR image and the slices of nonperiodic ISRJ. (**d**–**f**) The interfered ISAR image and the slices of APE.

Figure 14 illustrates the radar images generated by two jamming methods using the same transmission peak power. As depicted in Figure 14c,f, the peak of the jamming produced by the ISRJ method is significantly higher than that of the proposed method. However, after the jamming energy of the ISRJ method is processed by ISAR imaging, it is primarily concentrated in the direction and range of the jammer. Despite this, most of the plane features can still be successfully observed by the radar. A comparison of the HRRP and azimuth slices of Figure 14a,b with Figure 14d,e reveals that the jamming produced by the ISRJ method remains concentrated in the direction and range of the jammer. Particularly at the jammer's coordinate point, a peak is produced, consuming a substantial amount of jamming signal power. When the coordinate position is distant from the corresponding direction and range, the two-dimensional jamming power produced by ISRJ drops sharply and is much lower than the power produced by the proposed method. Therefore, under the same peak power limit, the proposed method's regional coverage effect is significantly superior to the ISRJ method. The jamming can completely cover the Area of Interest (AOI), and the energy distribution is uniformly spread.

Table 2 shows the quantitative analysis results obtained through 100 Monte Carlo simulations under different PJSR conditions. The JSR of the AOI in the output image reflects the efficiency of converting the jamming signal to the image. In the simulation, both the range and azimuth duty cycles set for ISRJ are 0.5, resulting in the total power of the ISRJ signal being 6 dB lower than the proposed method. In the three scenarios set, since the actual jamming is strip-like, the jamming power produced by ISRJ in the image is more than 50 dB lower than the proposed method. The proposed method demonstrates a far superior jamming energy conversion capability compared to ISRJ. In terms of image information quantity, the image entropy of ISRJ is close to the original image value of 6.8857 under three jamming power conditions, while the proposed method results in an entropy increase of about 1.1 to 1.3. In comparison with ISRJ, the proposed method introduces more redundant image information into the radar image.

Table 2. Comparison of the average performance of the proposed method with the classical method of ISRJ.

Setting	PJSR (dB)	Output JSR (dB)		Image Entropy	
		APE	ISRJ	APE	ISRJ
scene1	3	12.55	−52.23	8.1520	6.8859
scene2	−3	6.62	−52.69	8.1241	6.8876
scene3	−9	0.99	−53.57	7.8802	6.8886

From the perspective of the jamming mechanism, the proposed method offers greater flexibility in controlling the value and position of peak points in imaging through segment phase modulation. This addresses the issue of the strong scattering point at the jammer position in the radar image, resulting in a more uniform energy distribution in AOI.

Based on the analysis above, the proposed APE method outperforms the ISRJ method in terms of jamming energy conversion rate and regional jamming performance in radar two-dimensional images. However, the proposed method also places higher demands on the jamming modulation equipment while achieving improved jamming performance. From an engineering implementation perspective, ISRJ only requires selective forwarding, while APE requires the application of digital phase shifters to modulate the received radar signals in segments. Achieving a larger suppression range requires a shorter phase switching time of the phase shifter. According to the ISAR imaging mechanism, this indicator mainly depends on the range encoding width. On the other hand, when designing the encoding method with optimization criterion, the degree of freedom of encoding largely determines the number of iterations and calculations in the optimization. The encoding freedom of the ISRJ method is $2^N \times 2^{N_A}$. According to the duty cycle setting, the solution space of this sequence will be further reduced. In contrast, the APE has $L^N \times L^{N_A}$ kinds of coding sequences, and when the coding number is greater than 2, the iterative calculation amount of the APE method will be significantly greater than that of ISRJ. Therefore, the application of the method is dependent on further improvements in hardware capabilities.

5. Conclusions

In this research, an ISAR image feature suppression method based on 2D arbitrary phase encoding and GA coding sequence optimization is proposed. Increasing the phase modulation number and jamming power enhances the effectiveness of jamming in the feature suppression of the TOI. The guidelines for coding parameters design have been given. The APE method overcomes the issue of energy aggregation in stripe-shaped regions in 2D ISRJ. Experiments have proved that when the PJSR is higher than 0 dB, the target's scattering structure can be effectively masked. With the proposed optimization criteria, the image entropy of the interfered image increased by 1.1 to 1.5 compared to the original image.

The proposed optimization method primarily relies on radar signal parameters during iterations, making it straightforward to implement in engineering applications. Meanwhile, the technique provides a generalized solution rather than an optimal one for specific targets. Future research will incorporate target features into the jamming design and explore intelligent electronic countermeasures. The simulations in this experiment are conducted under the condition where the radar does not employ any anti-jamming measures. In real countermeasure scenarios, radars typically adopt anti-jamming techniques to mitigate jamming. Therefore, the jamming performance of the APE method in such countermeasure scenarios still requires further investigation. In addition, the application of the proposed optimization algorithm still faces the challenge of high computational complexity, and further research is needed to apply faster algorithms and optimization criteria.

Author Contributions: Conceptualization, S.X. and F.Z.; methodology, Q.W. and Y.W.; software, X.L., Q.W. and Y.W.; validation, X.L. and Z.X.; formal analysis, Z.X. and Q.W.; investigation, Q.W. and X.L.;

resources, F.Z. and S.X.; data curation, X.L. and Q.W.; writing—original draft preparation, Y.W. and Q.W.; writing—review and editing, Q.W., F.Z. and Y.W.; visualization, Z.X. and Y.W.; supervision, S.X. and F.Z.; project administration, Q.W.; funding acquisition, Q.W. All authors have read and agreed to the published version of the manuscript.

Funding: This research was funded by the Natural Science Foundation of Hunan Province under Grant 2022JJ40561, and the Scientific Research Program of National University of Defense Technology under Grant ZK22-46.

Data Availability Statement: The data presented in this study are available on request from the corresponding author due to privacy concerns.

Acknowledgments: The authors would like to thank the reviewers of this article. Their suggestions helped enrich the content of the article and improve the integrity and persuasiveness of it. At the same time, the authors are also very grateful to the editors of MDPI. Their careful modification of the article makes the expression of the article more accurate.

Conflicts of Interest: The authors declare no conflicts of interest.

References

1. Zou, X.; Jin, G.; He, F.; Zhang, Y. A New Waveform Design Method for Multi-Target Inverse Synthetic Aperture Radar Imaging Based on Orthogonal Frequency Division Multiplexing Chirp. *Remote Sens.* **2024**, *16*, 308. [CrossRef]
2. Anger, S.; Jirousek, M.; Dill, S.; Peichl, M. Inverse Synthetic Aperture Radar Imaging of Space Targets Using Wideband Pseudo-Noise Signals with Low Peak-to-Average Power Ratio. *Remote Sens.* **2024**, *16*, 1809. [CrossRef]
3. Zhang, H.; Liu, W.; Zhang, Q.; Liu, B. Joint Customer Assignment, Power Allocation, and Subchannel Allocation in a UAV-Based Joint Radar and Communication Network. *IEEE Internet Things J.* **2024**, *11*, 29643–29660. [CrossRef]
4. Wang, X.; Li, B.; Chen, H.; Liu, W.; Zhu, Y.; Luo, J.; Ni, L. Interrupted-Sampling Repeater Jamming Countermeasure Based on Intrapulse Frequency–Coded Joint Frequency Modulation Slope Agile Waveform. *Remote Sens.* **2024**, *16*, 2810. [CrossRef]
5. Zhang, H.; Liu, W.; Zhang, Q.; Fei, T. A robust joint frequency spectrum and power allocation strategy in a coexisting radar and communication system. *Chin. J. Aeronaut.* **2024**, *37*, 393–409. [CrossRef]
6. Wang, J.; Feng, D.; Xu, Z.; Wu, Q.; Hu, W. Time-Domain Digital-Coding Active Frequency Selective Surface Absorber/Reflector and Its Imaging Characteristics. *IEEE Trans. Antennas Propag.* **2021**, *69*, 3322–3331. [CrossRef]
7. Liu, G.; Li, L.; Ming, F.; Sun, X.; Hong, J. A Controllable Suppression Jamming Method against SAR Based on Active Radar Transponder. *Remote Sens.* **2022**, *14*, 3949. [CrossRef]
8. Song, C.; Wang, Y.; Jin, G.; Wang, Y.; Dong, Q.; Wang, B.; Zhou, L.; Lu, P.; Wu, Y. A Novel Jamming Method against SAR Using Nonlinear Frequency Modulation Waveform with Very High Sidelobes. *Remote Sens.* **2022**, *14*, 5370. [CrossRef]
9. Wu, Q.; Xu, Z.; Liu, X.; Zhao, T.; Wang, Y.; Zhao, F. Synthetic Aperture Radar Image Transform Using Periodic-Coded Phase Modulation. *IEEE Geosci. Remote Sens. Lett.* **2024**, *21*, 4013505. [CrossRef]
10. Li, Y.; Liu, J.; Chen, H. ISAR Interference Method Based on Sinusoidal Phase Modulation. *Signal Process.* **2007**, *23*, 101–105. (In Chinese)
11. Jiang, J.; Wu, Y.; Wang, H.; Lv, Y.; Qiu, L.; Yu, D. Optimization Algorithm for Multiple Phases Sectionalized Modulation Jamming Based on Particle Swarm Optimization. *Electronics* **2019**, *8*, 160. [CrossRef]
12. Wang, H.; Jiang, J.; Pu, J.; Wu, Y.; Ran, D. Low Sidelobe Multi-phase Segmented Modulation Interference Method Based on Cosine Amplitude Weighting. *J. Syst. Eng. Electron.* **2021**, *43*, 3185–3193. (In Chinese)
13. Sun, J.; Wang, C.; Shi, Q.; Ren, W.; Yao, Z.; Yuan, N. Intelligent Optimization of Phase Modulation Waveform Based on Genetic Algorithm. *J. Syst. Eng. Electron.* **2022**, *33*, 916–923. (In Chinese) [CrossRef]
14. Xu, H.; Quan, Y.; Zhou, X.; Chen, H.; Cui, T.J. A Novel Approach for Radar Passive Jamming Based on Multiphase Coding Rapid Modulation. *IEEE Trans. Geosci. Remote Sensing.* **2023**, *61*, 5101614. [CrossRef]
15. Wang, J.; Feng, D.; Zhang, R.; Xu, L.; Hu, W. An Inverse Synthetic Aperture Radar Image Modulation Method Based on Coding Phase-Switched Screen. *IEEE Sens. J.* **2019**, *19*, 7915–7922. [CrossRef]
16. Lang, W.; Mei, S.; Liu, Y.; Zhou, F.; Yang, X. A Periodic Multiple Phases Modulation Active Deception Jamming for Multistatic Radar System. *IEEE Trans. Aerosp. Electron. Syst.* **2023**, *59*, 3435–3451. [CrossRef]
17. Yu, D.; Wu, Y.; Wang, H.; Jia, X. Study on Multi-phase Segmented Modulation Interference Method for Inverse Synthetic Aperture Radar. *J. Electron. Inf. Technol.* **2017**, *39*, 423–429. (In Chinese)
18. Shi, Q. Research on ISAR Interference Technology Based on Phase Modulation. Ph.D. Thesis, National University of Defense Technology, Changsha, China, 2019. (In Chinese).
19. Li, S.; Wang, J.; Fang, X.; Lu, G.; Li, M.; Chen, W.; Chen, C. Jamming of ISAR Imaging With Time-Modulated Metasurface Partially Covered on Targets. *IEEE Antennas Wirel. Propag. Lett.* **2023**, *22*, 372–376. [CrossRef]
20. Wu, Q.; Liu, X.; Xu, Z.; Zhao, F.; Gu, Z.; Xiao, S. Flexible blanket synthetic aperture radar jamming using joint frequency and phase modulation. *IET Radar Sonar Navig.* **2023**, *17*, 1129–1141. [CrossRef]

21. Wu, Q.; Zhao, F.; Wang, J.; Xu, Z.; Xiao, S. ISAR image feature control method based on phase coded modulation. *Syst. Eng. Electron.* **2023**, *45*, 1000–1007. (In Chinese)
22. Wu, Q.; Zhao, F.; Ai, X.; Liu, X.; Xiao, S. Two-Dimensional Blanket Jamming Against ISAR Using Nonperiodic ISRJ. *IEEE Sens. J.* **2019**, *19*, 4031–4038. [CrossRef]
23. Cao, P.; Xing, M.; Sun, G.; Li, Y.; Bao, Z. Minimum Entropy via Subspace for ISAR Autofocus. *IEEE Geosci. Remote Sens. Lett.* **2010**, *7*, 205–209. [CrossRef]
24. Srinivas, N.; Deb, K. Muiltiobjective Optimization Using Nondominated Sorting in Genetic Algorithms. *Evol. Comput.* **1994**, *2*, 221–248. [CrossRef]